Integrating Fiber Optic Strain Sensors into Metal Using Ultrasonic Additive Manufacturing

Adam Hehr[1], Mark Norfolk[1], Justin Wenning[1], John Sheridan[2], Paul Leser[3], Patrick Leser[3], John A. Newman[3]

(1st affiliation) Fabrisonic LLC, Columbus, Ohio 43221, USA. – corresponding author email ahehr@fabrisonic.com
(2nd affiliation) Sheridan Solutions LLC, Saline, MI 48176, USA.
(3rd affiliation) NASA Langley Research Center, Hampton, VA 23681, USA.

Abstract

Ultrasonic Additive Manufacturing (UAM), a rather new three-dimensional (3D) printing technology, uses ultrasonic energy to produce metallurgical bonds between layers of metal foils near room temperature. This low temperature attribute of the process enables integration of temperature sensitive components, such as fiber optic strain sensors, directly into metal structures. This may be an enabling technology for Digital Twin applications, i.e., virtual model interaction and feedback with live load data. This study evaluates the consolidation quality, interface robustness, and load sensing limits of commercially available fiber optic strain sensors embedded into aluminum alloy (AA) 6061. Lastly, an outlook on the technology and its applications is described.

Introduction

Real-time monitoring of engineering systems is improving speed, efficiency, and safety through enhanced operational decision making. Recently, real-time physical system monitoring has been combined with a virtual mathematical model of the system to increase decision making quality even further. This combined physical-virtual monitoring concept conceived within the US Air Force, called Digital-Twin, feeds real-time information from the engineering system into its virtual "twin" or mathematical model in a control loop like framework for operation decision making and outcome prediction [1-3]. Combination of the physical and virtual domains in the same framework reduces the need for overdesign (safety factors), enhances reliability, improves maintenance decisions, and revolutionizes safety. The Digital Twin approach is gaining traction quickly in the industrial sector as well through new products and designs [4, 5].

A key component of the Digital Twin paradigm is its physical sensors and sensor systems for monitoring and feedback to the virtual twin. Historically, such health monitoring concepts have been difficult to implement due to cost, high channel counts, data processing needs, computational power and memory, and sensors not measuring key events, i.e., the sensor robustness and placement is not adequate to measure the state of concern [6]. Consequently, state awareness or health monitoring systems which reduce data quantity, simplify processing, and that are robust in design are enabling large scale health monitoring. Fiber optic strain sensors or fiber Bragg gratings (FBGs) fall into this enabling sensor category.

FBGs are miniature in size, made of glass, can be multiplexed, are immune to electromagnetic radiation, and are interrogated remotely. They have been successfully embedded in polymeric composites to measure unseen strain and damage states [6, 7]. The small size of the cable makes

it minimally invasive to the structure. Utilizing FBGs with metallic structures has been limited to external mounting until recently with the advent of 3D printing. Even now, the high formation temperature of melt-based 3D metal printing technologies prohibits reliable FBG integration. Instead, the sensors crack from residual thermal stress [8]. Ultrasonic Additive Manufacturing (UAM), a low temperature 3D metal printing technology, overcomes these formation challenges and has successfully been used to build FBGs into metal components for monitoring purposes [9, 10]. The incorporation of these sensors into the structure allows load states to be measured real-time in localized regions, which allows a reduction in the engineering safety factor and, ultimately, weight of the component.

Ultrasonic Additive Manufacturing (UAM) is a metal additive manufacturing process which involves building up a solid metal part through ultrasonically welding a succession of metal tapes. Periodic machining operations are used interchangeably with the ultrasonic welding stage to introduce internal features and to finalize geometry of the part [11]. Ultrasonic metal welding works by frictionally vibrating the metal surfaces together below their melting point resulting in an interfacial fusing of the materials [12]. This "scrubbing" action generates heat on a localized level near the interface—near 150^{o}C for aluminum and copper alloys [13]. Because melting is not the mechanism for joining, controlled atmospheres are not required for the process and solidification microstructures are absent. These attributes enable technology scale-up for large parts with predictable properties.

A commercial UAM system is shown in Figure 1(a) while the additive and subtractive stages are shown in Figure 1(b) and Figure 1(c) respectively. This UAM system has a build envelop near 2m x 2m x 1m. The control variables for the additive stage are welder vibrational amplitude (given typically in peak-to-peak amplitude), down force, translational travel speed, and an optional anvil pre-heat temperature. These control variables are shown in Figure 1(b). The scrubbing action is created through two high power ultrasonic transducers actuating the weld tooling, more commonly called the "sonotrode." The two transducers are operating in a push-pull configuration to enhance the energy delivery during the process [14].

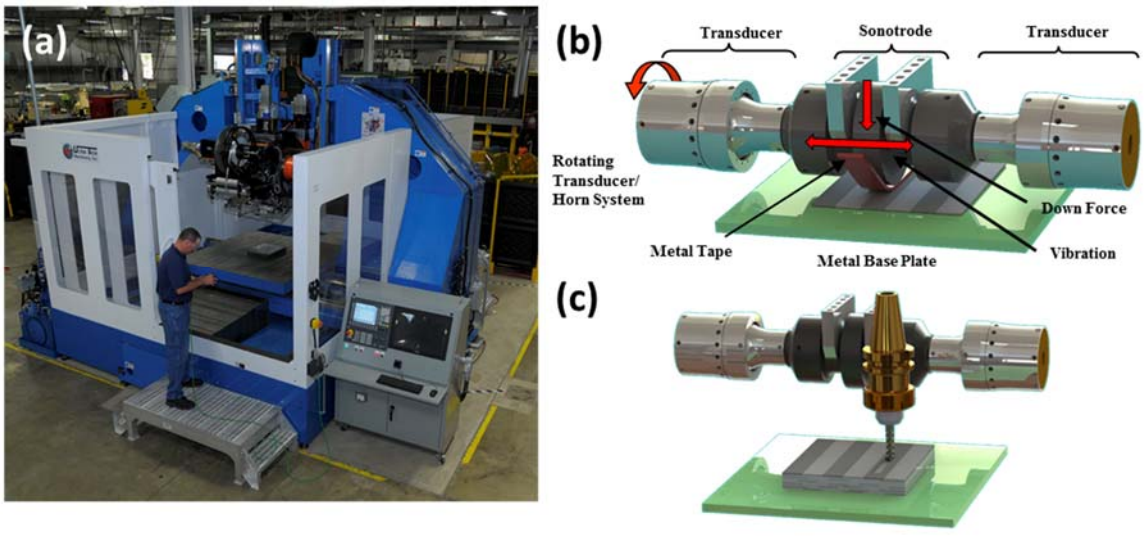

Figure 1. UAM process: (a) Fabrisonic SonicLayer™ 7200; (b) additive or ultrasonic welding stage of process; (c) subtractive or machining stage of process. Reproduced with permission [15].

The solid-state, non-melting nature of UAM enables the integration of temperature sensitive components into the metal structure directly without damage, i.e., sensors. Furthermore, the subtractive stage of the process allows accurate sensor placement within the structure during construction. As a result, metallic materials integrated with localized sensor placement becomes possible. The goal of this study was to understand the process required to embed FBG sensors with Ormocer® (organic modified ceramic) coatings, and to benchmark the strain sensing limits of these embedded strain sensors through tensile testing prescribed by ASTM standard E8. Finally, an outlook of the technology is described through examples of structures with embedded FBGS for NASA's Digital Twin program.

Sample Construction

Ormocer® coated FBGs were obtained from FBGS[1] for this research. Ormocer® is a stiff plastic coating that enables linear strain transfer to the glass fiber between -180 to 200°C [16]. With this coating, the fiber diameter is approximately 195 µm. The fiber optic cables used in this research have five independent grating sensors physically spaced 20 mm apart with grating lengths about 10 mm.

Prior to embedding the optical fiber, a slightly oversized channel was cut to enable location placement and to avoid sensor damage. The channel was cut to a 0.23 mm depth using a 0.25 mm four-flute ball nose end mill. The fiber was then placed into the cut channel and welded over with five layers of 0.15 mm thick AA 6061 H18 foil. The welding parameters used for encapsulation were a scrubbing amplitude of 32 µm peak-to-peak, a downforce of 4000 N, a translation speed of 4.44 m/min, and an ambient control temperature of 37.8°C. These welding parameters were selected from earlier pilot trials that demonstrated good consolidation quality around the fiber without damage to the fiber itself. These pilot trials confirmed a wide processing window, so parameters between extremes were selected in this study.

The strain or wavelength shift on the fiber during sample construction was measured to better understand consolidation behavior. FBG wavelength shift was recorded using a National Instruments PXIe system with a PXIe-4844 FBG card. Estimated strain response during construction was calculated using the literature gauge factor value, 0.78, for 1550 nm gratings [17]. Representative in-situ strain for one of the embedded FBGS is plotted in Figure 2. The residual strain per layer is shown in Figure 2(a) while the instantaneous strain during the welding of layer 5 is shown in Figure 2(b). For the first few layers, the sensor enters a compression state. The sensor then begins to measure a reduction in the compressive strain with additional layers. It is suspected that the initial compression state occurs from the sensor getting squeezed during consolidation. The squeezing action may occur from plastic flow of metal around the sensor. Plastic flow around embedded fiber like materials has been observed prior in UAM and the microstructures have been studied [18-21]. After the second layer of foil, the compressive state begins to decrease because the rolling action of the welder generates plastic strain within the part. The evolution of this cold work plastic strain is not well understood after layer 5 and requires further study, i.e., identify if or when cold work ceases.

[1] http://www.fbgs.com/

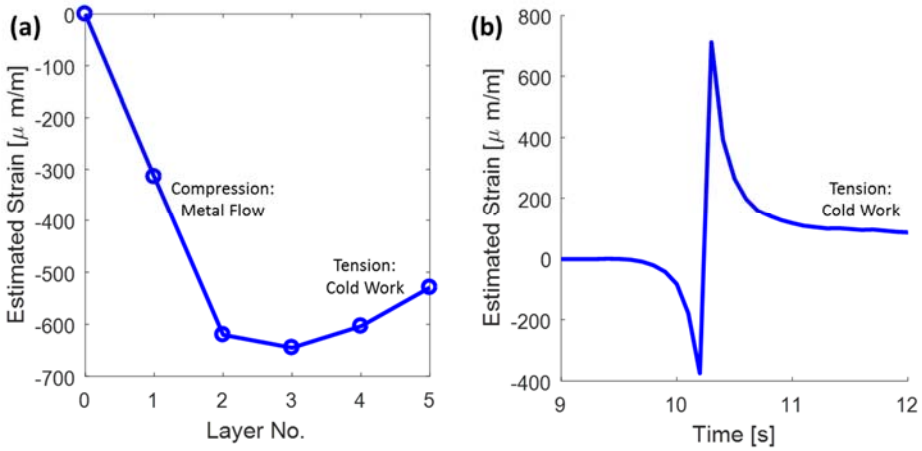

Figure 2. Strain behavior during sample construction: (a) strain accumulation as a function of welded layers; (b) dynamic strain during welding for fifth layer (zoomed-in for visibility). The first layers of welding impart a compressive strain on the fibers which is believed to be linked to metal flow around the fiber. On the other hand, later layers accumulate tensile cold work from the rolling action of the welder.

After layer addition, the subtractive stage of the UAM process was used to cut out tensile samples as prescribed in ASTM E8; see Figure 3(a). An exterior strain gauge was then added to the tensile sample for future comparative strain measurements and calibration. A representative cross-section of an embedded Ormocer® coated fiber is shown in Figure 3(b). The fiber was completely consolidated enabling reliable strain transfer to the glass fiber.

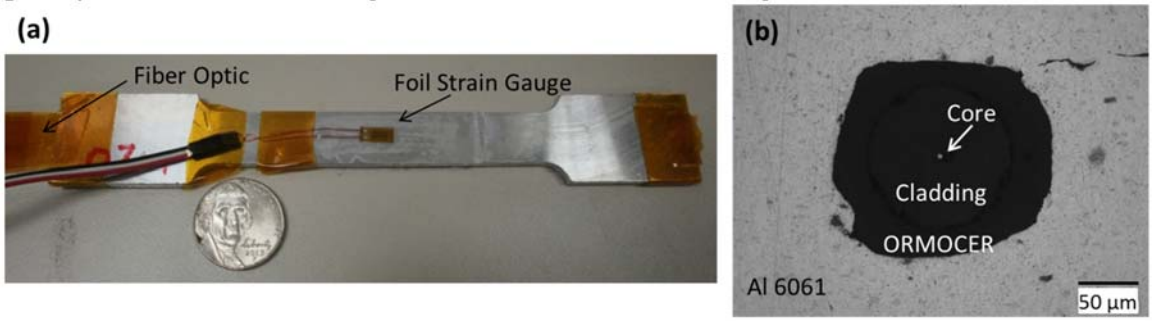

Figure 3. Embedded fiber optic strain sensors: (a) ASTM tensile sample used to evaluate strain sensing performance; (b) micrograph of representative consolidated fiber showing metal completely encapsulating the fiber.

Testing and Calibration

Three tensile samples were manufactured and tested in this study using the same materials and procedures. Each sample has five gratings or sensors, which enables study of fifteen data points. A single data trace is shown in this study that is representative of the total sample behavior.

To evaluate strain sensing limits as a function of load and for calibration purposes, cyclic tensile testing was carried out using a 20-kip MTS servohydraulic load frame. This testing was done at various stress levels using a 0.5 Hz sinusoidal waveform. Force and displacement were measured in addition to foil gauge strain and FBG strain. The same PXIe system was used to measure optical wavelength in this experiment. Foil gauge strain was measured using a PXIe-4330 strain card. The force and displacement were measured by recording calibrated voltage

outputs using a PXI-4462 voltage card. All measured waveforms were synchronized to the same sampling clock.

Correlated foil gauge strain and normalized FBG wavelength shift are shown in Figure 4(a) for a load level near half the ultimate tensile strength of AA 6061-T6 (157 MPa). The two quantities track each other qualitatively and do not demonstrate any noticeable divergence. The calibrated sensor gauge factors were found to be consistent at different stress levels. The calculated gauge factor values ranged between 0.705 and 0.72, which is less than 10% difference when compared to the published literature value of 0.78. These gauge factors were calculated using linear regression for a first order polynomial (straight line fit).

This tensile sample design creates a uniform axial strain field when stretched, since the sample was loaded solely in this direction. This axial strain field was equal on the outside and inside of the part. This strain equality was confirmed during testing by comparing the measured and theoretical gauge factor for the FBG. Although Poisson ratio effects create a lateral strain field in the sample, and ultimately a compressive stress or interface strain due to the materials having different Poisson ratios, the sensor will not measure this interface strain due to the fiber and aluminum having a fixed constraint in the axial direction (assuming perfect bonding). In practice, the external strain state may not be as easy to correlate to the internal strain state due to the presence of multi-axis loading and bending effects. In this case, sophisticated finite element models may be required to correlate the external and internal strain.

Strain-to-failure testing was used to evaluate the strain sensing limit of the embedded FBG, see Figure 4(b). The FBG and foil gauge exhibit linear correlation past the weld and baseplate material yield points, and diverges with the onset of plasticity in the sample. A sawtooth pattern was observed because the wavelength shift exceeds the set wavelength bounds in the interrogator – simply a signal processing limitation. Consequently, multiple sensors pass through a given wavelength band during testing. Some of the tested samples (not shown) demonstrated intermittent fiber pull-out after the aluminum broke. The fiber broke simultaneously with the aluminum in others. This failure region was outside the sensing limits of the interrogator.

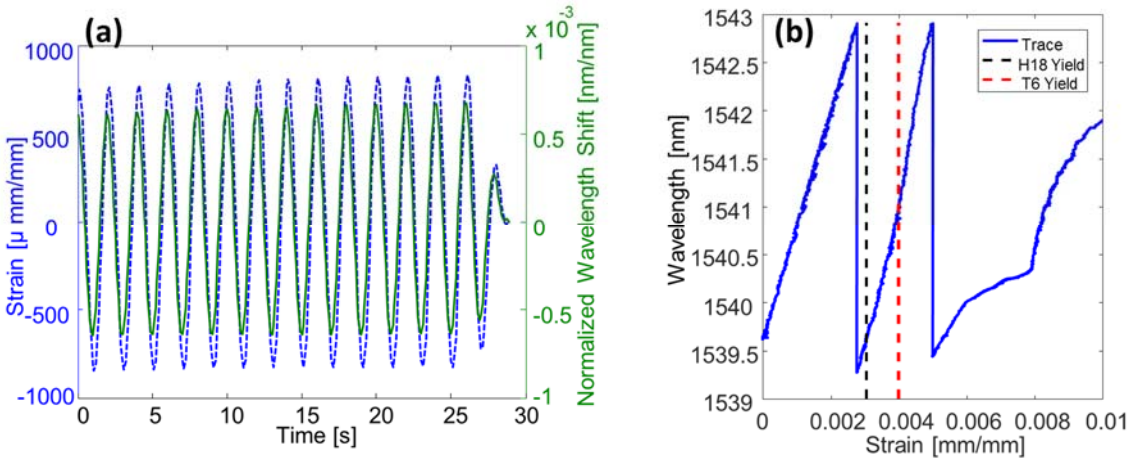

Figure 4. Tensile testing: (a) exterior strain and embedded FBG wavelength shift (not calibrated strain) cyclic profile comparison; (b) wavelength response vs. strain during strain limit testing. In (b), the embedded FBG tracks past the yield limit of the weld (H18) and baseplate (T6) materials. A sawtooth pattern is seen because the strain exceeds the set wavelength bounds in the interrogator for a given FBG as the sample is stretched. As a result, the strain from multiple FBGs are seen in the graph.

Summary and Technology Outlook

UAM was used to embed fiber optic FBG strain sensors into aluminum ASTM tensile samples. Concurrent with sample manufacture, the fiber strain was measured. The first few consolidation layers create a large compressive stress while later layers relieve some of this compressive stress through the consecutive rolling action of the welder. After the samples were built, quasi-static and cyclic tensile testing were used to evaluate strain sensing performance. The embedded sensors do not demonstrate slip behavior until after the yield point of the material, and their calibration is near literature values.

This fundamental work enabled the creation of more complicated structures for evaluation. Recently, the team built a fatigue specimen designed by NASA's Digital Twin project, see Figure 5(a). The specimen is designed such that failure is difficult to predict. This fatigue specimen is near 4" x 20" (10 cm x 51 cm) in size, exhibits complex geometry, and has 30 FBG sensors located around stress concentrators within the part. The team is also working toward enhancing the robustness of embedded fiber optic systems (see Figure 5(b)) and using metallized coatings to expand the temperature operation regime (see Figure 5(c)). Flight hardware is being developed with embedded sensors near critical stress points within the components.

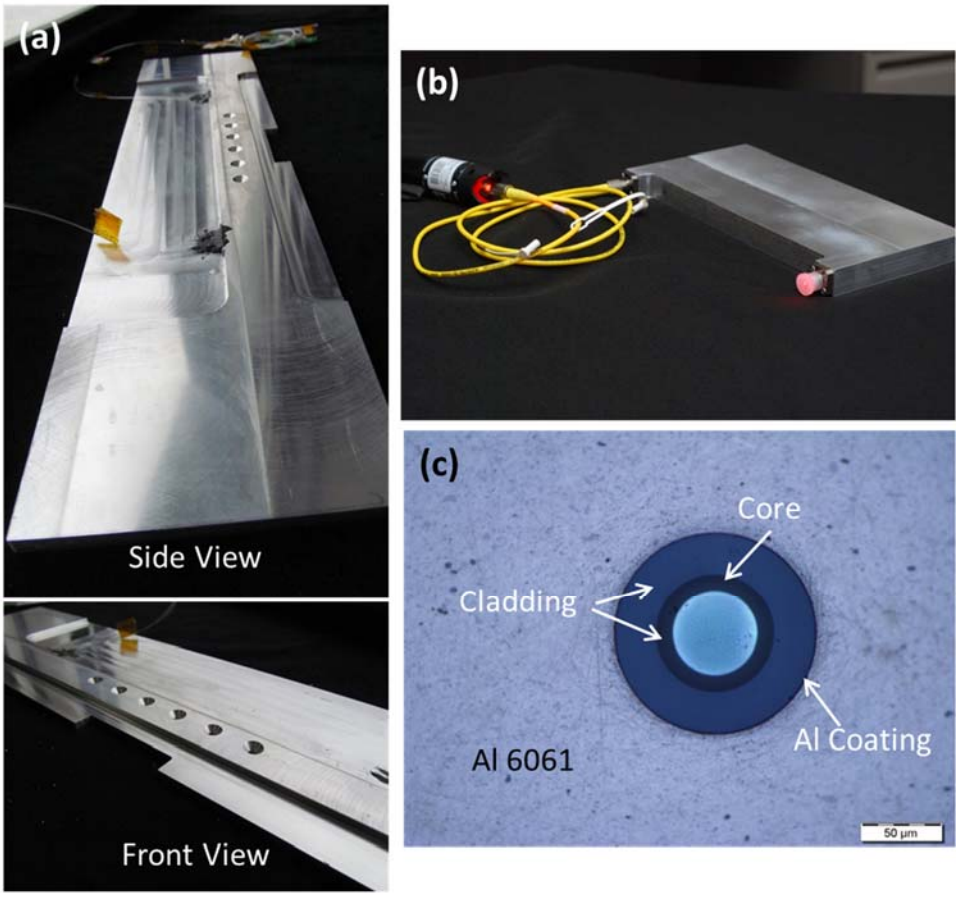

Figure 5. Outlook of technology: (a) Fatigue specimen developed by NASA's Digital Twin Project with 30 embedded FBG sensors near stress concentrators in the sample (see bolt holes and notch in front view); (b) embedded FBG connector for robustness; (c) metallized fiber optic cables to expand useable temperature range.

Acknowledgments

The authors would like to acknowledge financial support from NASA's SBIR Office, NNX16CL33C. The authors are grateful for the support of NASA's Convergent Aeronautics Solutions (CAS) Program Digital Twin Project.

References

[1] E. Tuegel, A. Ingraffea, T. Eason and S. Spottswood, *Int. J. Aerosp. Eng*., (2011).

[2] G. W. Hunter, D. E. Berger, J. D. Lekki, R. W. Mah, D. F. Perey, S. R. Schuet, D. L. Simon and S. W. Smith, Report No. 217825, NASA, Cleveland, OH, March 2013.

[3] E. H. Glaessgen and D. Stargel, *Proc. - AIAA/ASME/SAE Struct., Struct. Dyn., Mater. Conf.*, (2012).

[4] C. J. Parris, J. Laflen, M. Grabb and D. Kalitan, "The future for Industrial Services: The Digital Twin", https://www.infosys.com/insights/digital-future/Pages/future-industrial-digital.aspx. Accessed 22 August 2017.

[5] Siemens, "The digital twin," https://www.siemens.com/customer-magazine/en/home/industry.html. Accessed 2 October 2017

[6] D. Huston, *Structural Sensing, Health Monitoring, and Performance Evaluation*, 1st ed. (Boca Raton, FL: CRC Press, 2011), pp. 5-15

[7] K. Kuang and W. Cantwell, *Appl. Mech. Rev.*, 56, (2003).

[8] D. Havermann, J. Mathew, W. N. MacPherson, D. P. Hand and R. R. Maier, *Proc. SPIE*, (2015).

[9] C. Mou, P. Saffari, D. Li, K. Zhou, L. Zhang, R. Soar and I. Bennion, *Meas. Sci. Technol.*, 20, (2009).

[10] J. Schomer, A. Hehr and M. Dapino, *Proc. SPIE*, (2016).

[11] D. White, *Adv. Mater. Process.*, 161, 64 (2003).

[12] K. Graff, J. Devine, J. Keltos, N. Zhou and W. Roth, in *AWS Welding Handbook*, (2001), p 263.

[13] M. Sriraman, M. Gonser, H. Fujii, S. Babu and M. Bloss, *J. Mater. Process. Technol.*, 211, 1650 (2011).

[14] K. Graff, M. Short and M. Norfolk, *Solid Freeform Fabr. Symp. Proc.*, (2010).

[15] A. Hehr, J. Wenning, K. Terrani, S. S. Babu and M. Norfolk, *JOM*, 69, 485 (2017).

[16] FBGS, "Ormocer Coating," http://www.fbgs.com/technology/why-we-have-chosen-to-use-an-ormocer-coating/. Accessed 23 August 2017.

[17] M. Kreuzer, "Strain Measurement with Fiber Bragg Grating Sensors," https://www.hbm.com/en/3189/tips-and-tricks-strain-measurement-with-fiber-bragg-grating-sensors/. Accessed 2 October 2017.

[18] C. Kong and R. Soar, *Appl. Opt.*, 44, 6325 (2005).

[19] D. Li and R. Soar, *J. Mater. Sci. Eng. A*, 498, 421 (2008).

[20] R. Friel and R. Harris, *Proc. Inst. Mech. Eng., Part L*, (2010).

[21] A. Hehr and M. Dapino, *Composites, Part B*, 77, 199 (2015).